Zentrum für Technomathematik

Fachbereich 3 – Mathematik und Informatik

Taylor-Couette System with Asymmetric Boundary Conditions

Eberhard Bänsch **Christoph Egbers**
Oliver Meincke **Nicoleta Scurtu**

Report 00–04

Berichte aus der Technomathematik

Report 00–04 **Februar 2000**

Taylor-Couette System with Asymmetric Boundary Conditions

Oliver Meincke[1], Christoph Egbers[1], Nicoleta Scurtu[2], and Eberhard Bänsch[2]

[1] ZARM, Center of Applied Space Technology and Microgravity, University of Bremen, Am Fallturm, 28359 Bremen, Germany
[2] Center of Technomathematics, University of Bremen, Postfach 33 04 40, 28334 Bremen, Germany

Abstract. We report on a study on stability, bifurcation scenarios and routes into chaos in Taylor-Couette flow. By increasing the Reynolds number with the angular velocity of the driving inner cylinder, the flow bifurcates from laminar mid-plane-symmetric basic flow via a pitchfork bifurcation to mid-plane-symmetric Taylor-Vortex flow. Both flow states are rotationally symmetric. We now compare the dynamical behaviour in a system with symmetric boundary conditions with the effects in an asymmetric system. We also could vary the gap widths. The different flow states can be detected by visualization with small aluminium flakes and also measured by Laser Doppler Velocimetry (LDV) and Particle Image Velocimetry (PIV). The dynamical behaviour of the rotating flow is discussed by time series analysis methods and velocity bifurcation diagrams and then compared with numerical calculations.

1 Introduction

The subject of hydrodynamic instabilities and the transition to turbulence is important for the understanding of nonlinear dynamic systems. A classical system to investigate such instabilities is besides the Rayleigh-Bénard system the Taylor-Couette system. The system was first examined theoretically and experimentally by Taylor [16]. It consists of two concentric cylinders where the so formed gap is filled with the working fluid. Here, only rotation of the inner cylinder is considered and the outer one is held at rest. By increasing the speed of the inner cylinder, the azimuthal Couette-flow becomes unstable and is replaced by a cellular pattern in which the fluid travels in helical paths around the cylinder in layers of vortices (Taylor-Vortex flow). By a further increase of the rotation speed the system undergoes several bifurcations before the flow structure becomes more complicated. Different routes to chaos are possible by further increasing the rotation rate. One model was described by Ruelle & Takens [13]. Benjamin [3], [4] showed the importance of the finite size of the cylinders and its effects upon the bifurcation phenomena. A summary of the current state of research was published by Ahlers [1], Chossat [6], Koschmieder [9], Meyer-Spasche [10] und Tagg [15].

In this work, short systems are investigated to reduce the multiplicity of possible solutions. Some new aspects of the dynamical behaviour of the Taylor-Couette flow during the transition to turbulence for the case of symmetric and

asymmetric boundary conditions and the small ($\eta = 0.85$) and the wide gap width ($\eta = 0.5$) are presented in this study.

2 Experimental setup

Most of our experiments were carried out by increasing the Reynolds number of the inner cylinder in a quasistationary way from rest. However, since the occuring flow structures could depend on initial conditions, it is possible to vary the acceleration rate for the cylinder. The temperature was precisely controlled and measured to allow the determination of a well defined Reynolds number of the flow. The Taylor-Couette flow is characterized by the following three control parameters: The aspect-ratio ($\Gamma = H/d$), the radius ratio ($\eta = R_i/R_a$) and the Reynolds number $Re = \frac{R_i d \Omega_i}{\nu}$, where H, d, R_i, R_a, Ω_i and ν are the height, the gap width, the inner and outer radii, the angular velocity of the inner cylinder and the kinematic viscosity respectively. The symmetric experimental setup is illustrated in Fig. 1a. It is only possible to obtain different aspect ratios by integrating different inner cylinders due to the constant length of the system. The radius ratios we used during this work were ($\eta = 0.5$) to realize a wide cylindrical gap and ($\eta = 0.85$) a small one. To realize asymmetric boundary conditions, a new setup consisting an inner cylinder with a mounted bottom plate is available (Fig. 1b). In this system the radius ratio is ($\eta = 0.5$) and the aspect ratio is variable.

3 Measuring Techniques

To observe the behaviour of the flow, two different techniques were used. Using the PIV-technique one gets a 2–D vector map of the flow field whereas LDV yields to time series with high resolution containing information about one component of velocity at a special location in the working fluid depending on time.

3.1 PIV

In our system a pulsed double cavity, frequency doubled Nd:YAG-Laser is used for the **P**article **I**mage **V**elocimetry. The second cavity is required to get a very short time delay between the two pulses. A single laser achieves only a repetition frequency of about 15Hz. This time delay is too long for high flow rates and no correlation between the records would be possible. The emitted laser beam is frequency doubled and then spread with a cylindrical lense to get a green light sheet, because the original wavelength of a Nd:YAG-Laser is in the infrared spectrum. To get two images in a short time-interval, a fast CCD-camera is used. In Fig. 2 a sketch of the Taylor-Couette system with the applied PIV-setup is shown. With the two recorded images one gets a light intensity distribution which shows the particles suspended into the measuring fluid. The recorded images are devided into smaller subareas, so called 'interrogation areas'. The

a) photograph of the symmetric experimental setup

b) principle sketch of the asymmetric setup with rotating bottom plate

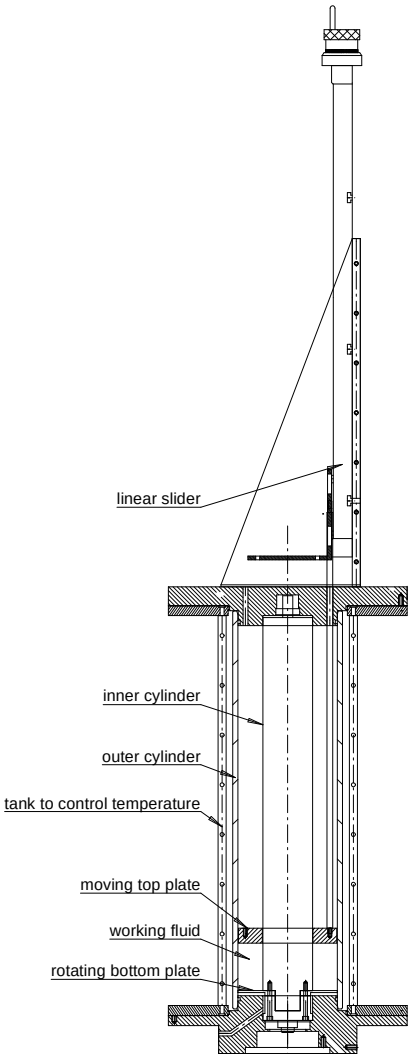

Fig. 1. *The two different experimental setups which were used during this work*

cross correlation algorithm (see Eqn. 1) calculates for every interrogation area a vector of the movement of the particles so that at least a 2-D vector map of the

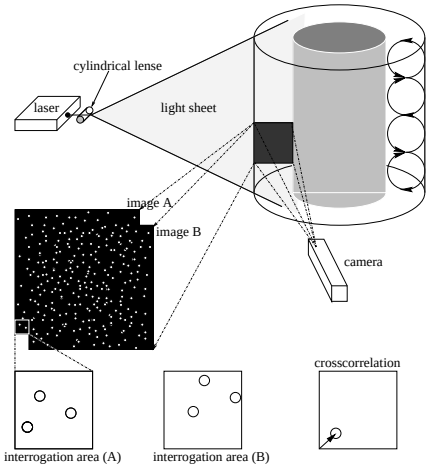

Fig. 2. *Taylor-Couette system with the applied PIV-setup*

flow in the gap is illustrated.

$$\sum\sum I(m,n)I^{\star}(m+i,n+j) = \mathcal{C}(i,j) \tag{1}$$

I and $I^{\star}$ describe the light intensities within the interrogation areas at the time t and Δt due to the spatial coordinates m and n. The crosscorrelation $\mathcal{C}(i,j)$ has its maximum, if many particles correlate with their spatial shifted equivalent $\rightarrow$ true correlation. To get more information about the PIV-technique the reader is refered to the book by Raffel et al. [11].

3.2 LDV

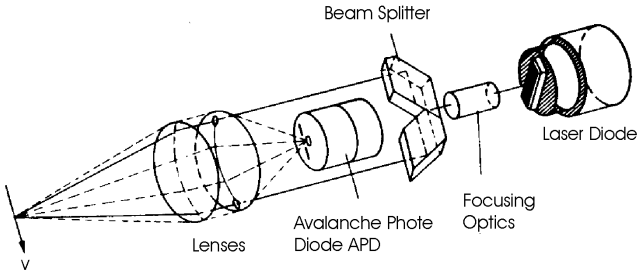

Fig. 3. Sketch of LDV, [12]

Laser-**D**oppler-**V**elocimetry is a widely accepted tool for fluid dynamic investigations, as it gives information about flow velocity without influencing the fluid.

For the application of the Laser-Doppler-Velocimetry on the rotating system a special traversing system has been constructed, which allows the traversing of the LDV-system in axial direction. Fig. 3 shows a principle sketch of a LDV-system. The LDV-system used in our experiments consists of a He-Ne-Laser, whose beam is split and then one laser beam is shifted in its frequency. Suspended particles create a signal by scattering light when passing the interference fringes formed by the intersected beams in the measuring volume. From these Doppler Bursts information of the direction and the quantity of the velocity can be obtained. As tracer particles for the LDV-measurements polysterene spheres with a diameter of 1.6µm were used. By using different algorithms, for example described in [18], it is possible to calculate the power spectrum, the attractors and bifurcation diagrams out of the obtained time series, measured with the LDV-system. Both systems we used are distributed by DANTEC-Electronics, Denmark

4 Numerical Method

The mathematical model to describe the system are the incompressible Navier–Stokes equations. Since we are mainly interested in the first bifurcations and to limit the required cpu–times, we use a 2.5–D approach. This means we assume that all dependent variables are constant in the azimuthal direction φ. Numerical computations for the full 3–D problem will be reported in a forthcoming paper.

The 2.5–D incompressible Navier–Stokes equations read in dimensionless form: We are looking for a velocity field $\boldsymbol{u} = u_r \boldsymbol{e}_r + u_z \boldsymbol{e}_z + u_\varphi \boldsymbol{e}_\varphi$ and a pressure field p fulfilling

$$\begin{aligned}
\partial_t u_r + u_r \partial_r u_r + u_z \partial_z u_r - \frac{1}{r} u_\varphi^2 &= -\partial_r p + \frac{1}{Re}\big(\frac{1}{r}\partial_r(r\partial_r u_r) + \partial_z^2 u_r - \frac{1}{r^2} u_r\big) \\
\partial_t u_z + u_r \partial_r u_z + u_z \partial_z u_z &= -\partial_z p + \frac{1}{Re}\big(\frac{1}{r}\partial_r(r\partial_r u_z) + \partial_z^2 u_z\big) \\
\partial_t u_\varphi + u_r \partial_r u_\varphi + u_z \partial_z u_\varphi + \frac{1}{r} u_r u_\varphi &= \frac{1}{Re}\big(\frac{1}{r}\partial_r(r\partial_r u_\varphi) + \partial_z^2 u_\varphi - \frac{1}{r^2} u_\varphi\big)
\end{aligned}$$

$$\frac{1}{r}\partial_r(r u_r) + \partial_z u_z = 0$$

for $t > 0$, $\frac{\eta}{1-\eta} = r_i < r < r_a = \frac{1}{1-\eta}$, $0 < z < \Gamma$ and $0 \le \varphi < 2\pi$ together with the no–slip boundary conditions

$$\begin{aligned}
&u_r = u_z = 0, \quad u_\varphi = 1 && \text{at } r_i = \frac{\eta}{1-\eta} \\
&u_r = u_z = u_\varphi = 0 && \text{at } r_a = \frac{1}{1-\eta} \\
&u_r = u_z = 0 && \text{at } z = 0 \quad \text{and } z = \Gamma
\end{aligned}$$

and either

$$u_\varphi = 0 \qquad \text{at } z = 0 \quad \text{and } z = \Gamma \qquad \text{(symmetric case)}$$

or

$$u_\varphi = r\frac{1-\eta}{\eta} \quad \text{at } z = 0 \quad \text{and } u_\varphi = 0 \quad \text{at } z = \Gamma \qquad \text{(asymmetric case)}.$$

Here we have used dimensionless velocities, pressures and coordinates.

To solve this problem numerically, we use a code based on the method described in [2] and in [17] for the 2.5–D case. The method uses the so called *fractional step θ–scheme* for the time discretization in a variant as an operator splitting to decouple the incompressibility condition from the nonlinearity, see also [8]. For the space discretization the *Taylor–Hood* element, i.e. piecewise quadratic finite elements for the velocity and piecewise linears for the pressure, are used.

5 Results

5.1 Symmetric system

In this section the influence of the gap width on the flow is investigated. On this account experiments on bifurcation scenarios in the Taylor-Couette system were carried out for two different radius ratios, $\eta = 0.85$ (small gap) and $\eta = 0.5$ (wide gap). The velocity bifurcation diagrams as illustrated in Fig. 4 and 5 were obtained by collecting the extrema of the velocity time series measured with the LDV-technique with a quasi-stationary increase of the Reynolds number. As it can be seen from the bifurcation diagram (Fig. 4), the flow undergoes a bifurcation from the laminar basic state to a steady Taylor vortex flow via a pitchfork bifurcation. This is an imperfect pitchfork bifurcation perturbed by the boundary conditions. By smoothly increasing the Reynolds number only one branch is reachable, which is the normal mode with inward flow adjacent to the end plates. The anomalous mode may be reached by changing the Reynolds number instantaneously. After this pitchfork bifurcation, the flow bifurcates via a Hopf bifurcation into the Wavy-Mode. With a further increase of the Reynolds number, the flow bifurcates via a second Hopf bifurcation into the modulated wavy mode before chaotic motion occurs. The second critical Reynolds number for the onset of the wavy mode is about 2.5 times higher as the first critical one. In contrast to small cylindrical gaps ($\eta = 0.85$) just mentioned, the experiments on bifurcation scenarios in the wide gap Taylor-Couette system $\eta = 0.5$ show a different bifurcation scenario and a different route into chaos, which is illustrated in Fig. 5. The basic flow bifurcates via a pitchfork bifurcation into Taylor vortex flow. The onset of the Wavy-Mode is shifted to higher Reynolds numbers in comparison to $\eta = 0.85$ because the vortices at the end-plates cannot oscillate due to the boundary conditions. This state is only stable over a small range of Reynolds numbers and it seems that the flow bifurcates directly into chaotic motion.

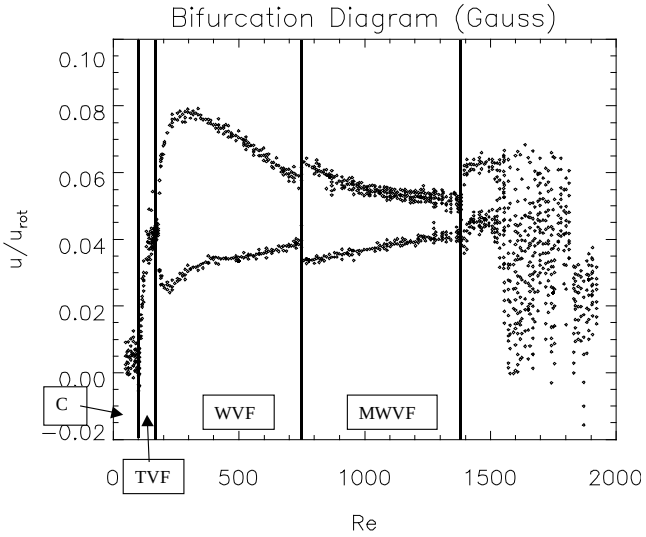

Fig. 4. *Bifurcation diagram in the Taylor-Couette system as a function of the Reynolds number. The meridional velocities are normalized by the velocity of rotation* ($\eta = 0.85$, $\Gamma = 13.2$, $z = 0.40L$, $(r - R_i)/(R_a - R_i) = 0.6$)
C: Couette flow *TVF: Taylor-Vortex flow* *WVF: Wavy-Vortex flow*
MWVF: Modulated Wavy Vortex flow

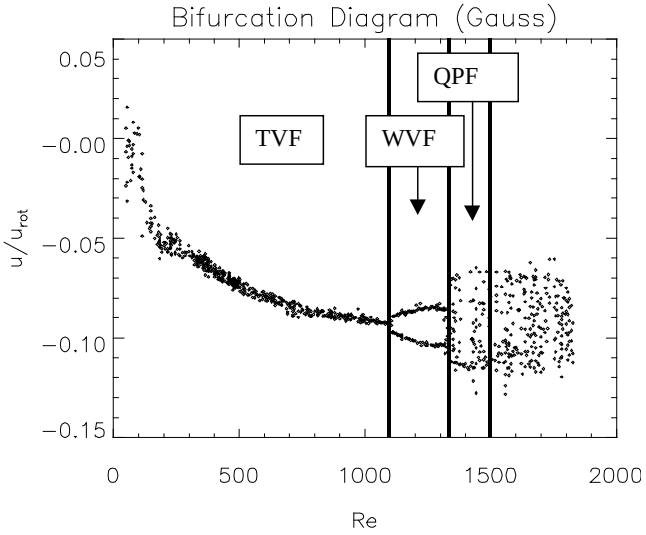

Fig. 5. *Bifurcation diagram in the Taylor-Couette system as a function of the Reynolds number. The meridional velocities are normalized by the velocity of rotation.* ($\eta = 0.5$, $\Gamma = 3.97$, $z = 0.37L$, $(r - R_i)/(R_a - R_i) = 0.91$)
TVF: Taylor-Vortex flow *WVF: Wavy-Vortex flow*
QPF: Quasiperiodic flow

a)

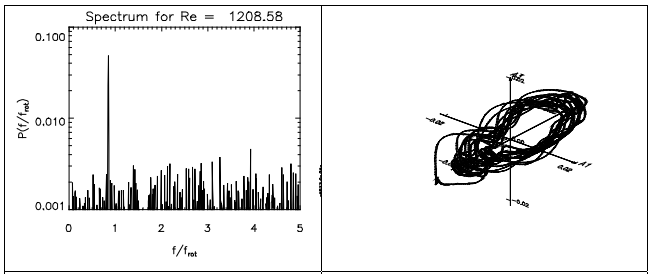

$Re = 1220$

b)

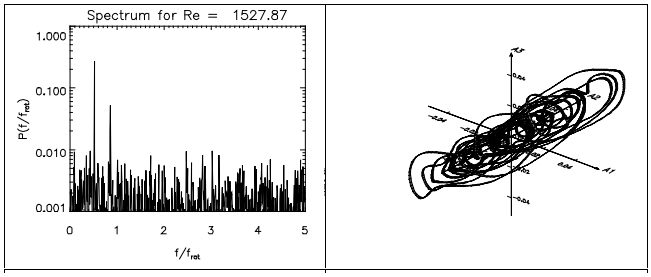

$Re = 1500$

Fig. 6. *powerspectrum and attractor in case of two different Reynolds numbers* ($\eta = 0.5$, $\Gamma = 3.97$, $z = 0.37L$, $(r - R_i)/(R_a - R_i) = 0.91$)

Figure 6 shows the frequency spectrum and the attractor for two different Reynolds numbers. The spectrum of Fig. 6a shows one characteristic frequency. All diagrams correspond to the Wavy vortex flow state. The reconstruction of the flow yields a limit cycle which is perturbed by noise. In the flow state in Fig. 6b a second frequency occurs at higher Reynols numbers. The attractor is not a limit cycle anymore. It is pointed out that it is a quasiperiodic flow state and not a chaotic one. The further research is now focussed on the exact investigation of the dynamics of Reynolds numbers higher than Re = 1500.

In Fig. 7 three experimental flow states obtained with the PIV-technique are shown. Fig. 7b shows the normal 4-vortex state which could be reached by increase the Reynolds number in a quasistationary way. Figs. 7c and 7d represent the two different anomalous modes which could be obtained in this system with a constant $\Gamma = 3.97$. These two flow states could be adjusted by a sudden increasing of the Reynolds number. In contrast to the stretched 3-vortex state the 5 vortices are squeezed into the system. In comparison with the experimental results a normal flow state is calculated and shown in 7a. The cores of the vortices are shifted to the outer cylinder but not as much as in the experimental result. In the experiment the cores seem to be closer to the outer cylinder due to the optical

way through curved surfaces with different refraction indices. This distortion is reduced in the new experimental setup using a rectangular tank filled with silicon oil enclosing the whole setup, which in addition keeps the working temperature constant.

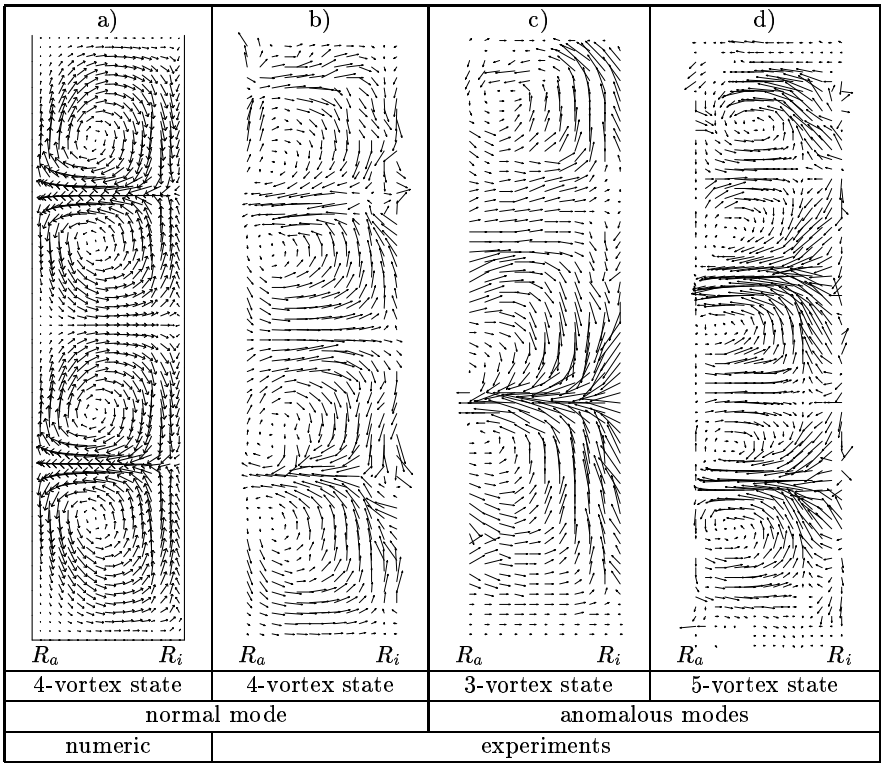

Fig. 7. Experimental and numerical results in case of the following parameters: $\eta = 0.5$, $\Gamma = 3.97$ and $Re = 500$. Experimental results obtained by using different acceleration rates.

To investigate the influence of the boundary conditions in the Taylor-Couette system an asymmetric experimental setup with a rotating bottom plate was constructed. First results are described in Section 5.2.

5.2 Asymmetric system

In this section we also only consider the situation where the outer cylinder is held at rest and the inner rotates. In this part of our research the effects of end conditons should be investigated. In contrast to the previous Section the

bottom end plate is allowed to rotate with the inner cylinder. As a result of the rotating bottom plate always outward flow is found adjacent to the rotating plate, whereas at the stationary top plate inward flow occurs. This leads to an odd number of cells in such an experimental setup, when only normal modes are considered.

In 1986, Cliffe & Mullin [7] investigated both experimentally and numerically the interaction between 5-cell and 3-cell modes in the asymmtric system. They investigated the stability of the flow states in a range of $\Gamma = 4.2 - 5.0$ and $Re = 50 - 300$.

Stability of 3-cell and one cell modes

In 1997, Blohm [5] in coorperation with Mullin focussed his investigations on the 3-cell and 1-cell modes. One result of his work is the stability diagram of steady solutions shown in Fig. 8. The line between H and M represents the transition from steady 3-cell flow to steady one cell flow by numerical calculations. The experimental stability limit was investigated by smoothly increasing the Reynolds number at a fixed Γ. The squares between H and J indicate a transition from steady 3-cell flow to a time dependent 1-cell state. Beyond J up to K the system passes through a transition from steady 3-cell to steady 1-cell flow. A transition from steady 1-cell to steady 3-cell flow by decreasing the Reynolds number could only be found numerically at line HI. Experimentally, time dependence occurs by decreasing the Reynolds number at higher values so that the line from H to I could not be found in the experiments.

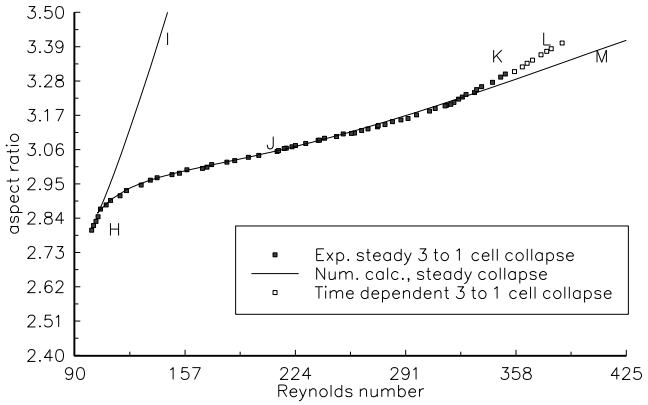

Fig. 8. Experimental and numerical stability diagram measured by Blohm [5] and calculated by Mullin

For comparison the stability limit between the 3-cell mode and the 1-cell mode was calculated during this work by the numerical method described in Sect. 4. In consideration of the fact that a 2.5–D-Code was used, no transitions to time

dependent states were found. The squares in Fig. 9 represent the transition from three vortices to one vortex by increasing the Reynolds number, whereas the circles indicate the change from 1-cell state to 3-cell state when decreasing the Reynolds number. Note that as mentioned before this line could not be reached experimentally due to the occurence of time dependence at higher Reynolds numbers. As an example of the two occuring flow states the calculated 3-vortex-

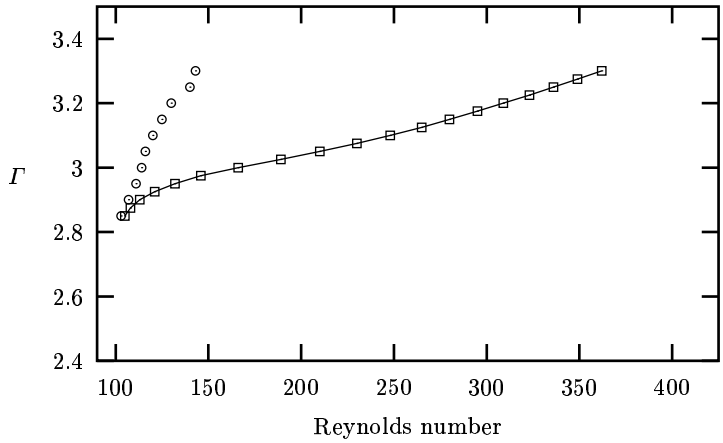

Fig. 9. *Numerical stability diagram, our computations. Squares represent the transition from three vortices to one vortex by increasing the Reynolds number. Circles indicate the change from 1-cell state to 3-cell state when decreasing the Reynolds number.*

and 1-vortex states are shown in Fig. 10 for $\Gamma = 3.2$ and two different Reynolds numbers. The visualization of the numerical results was realized with GRAPE [14]. The arrows represent the velocity components in r- and z-direction in the whole cylindrical gap. The inner cylinder on the left side and the bottom plate are rotating. The top plate and the outer cylinder on the right side are fixed.

Growth of bottom vortex

Blohm [5] found that the size of the cell adjacent to the rotating bottom plate is depending on the Reynolds number. For different Γ he experimentally investigated the size of the bottom vortex in percent of the height of the cylinder depending on the Reynolds number. The results are shown in Fig. 11 The effect of the growing bottom vortex could be seen clearer in the case of higher values of Γ.

To check these results, different flow states depending on the Reynolds number for two different Γ were calculated. Figure 12 and Fig. 13 show the development

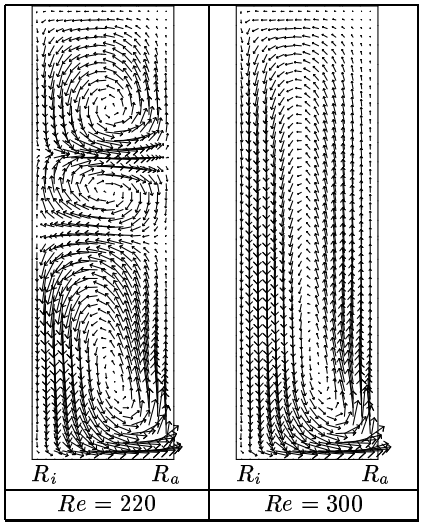

Fig. 10. *Numerical results for $\Gamma = 3.2$ Left side and bottom are rotating. The velocity components in r- and z-direction in the whole cylindrical gap are shown respectively, our computations.*

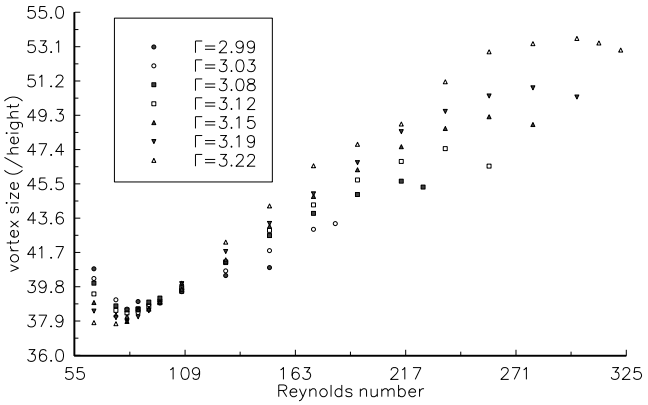

Fig. 11. *Experimental results for the growth of the bottom vortex depending on the Reynolds number due to different values of Γ.*

of the bottom vortex in the case of $\Gamma = 2.975$ and $\Gamma = 3.225$. These calculations confirm that in the case of a large Γ the effect of growing is considerably more noticeable.

Results by decreasing Re: $\Gamma = 3.15$

In this Section an example for the onset of a time dependent flow in the numerical calculations by decreasing the Reynolds number in the case of $\Gamma = 3.15$ is

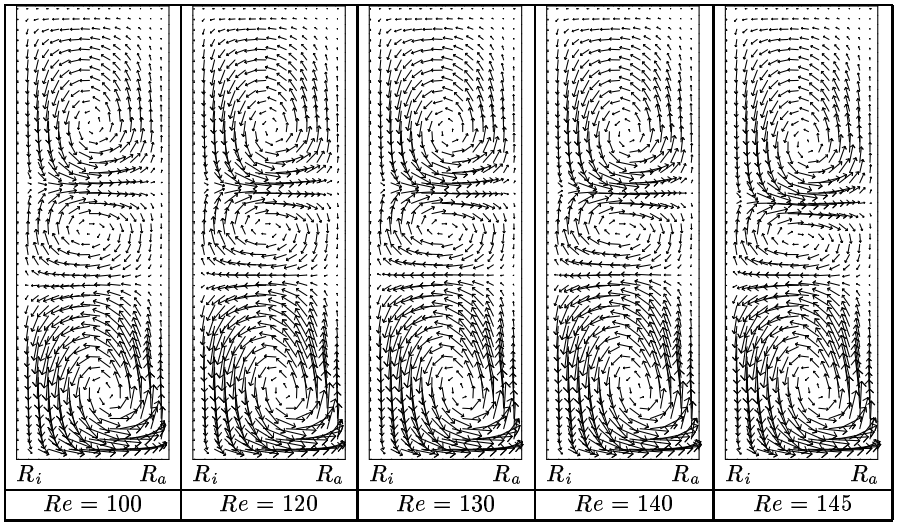

Fig. 12. *Numerical results for $\Gamma = 2.975$ depending on Re.*

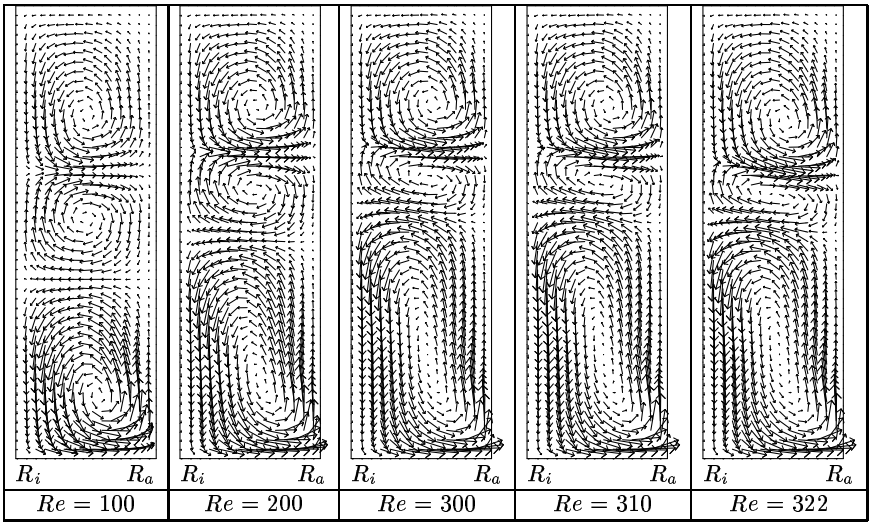

Fig. 13. *Numerical results for $\Gamma = 3.225$ depending on Re.*

shown. The two graphics in Fig. 14 represent the difference in the flow state in arbitrary units (a.u.) for consecutive time steps. Calculations at $Re = 173$ converge straightly so that a steady state is reached very fast. $Re = 172$ shows an oscillating behaviour in the difference which is an indication for an oscillating flow in the system although only a 2.5–D-Code was used. Blohm found these oscillations by decreasing the Reynolds number in his experiments.

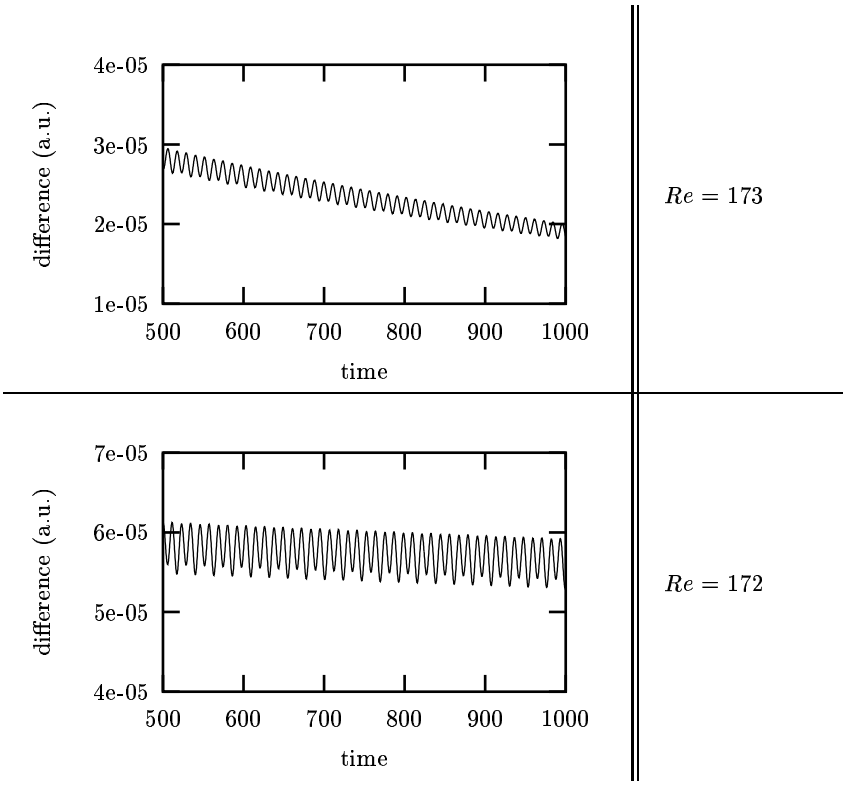

Fig. 14. *Difference between two calculated flow states at t and $t + \Delta t$ depending on time for two different Reynolds numbers*

6 Conclusions

In this work experimental and numerical investigations in consideration of different boundary conditions for the Taylor-Couette system are presented. First the experimental results in a very short annulus due to two different aspect ratios in the symmetric system were described. It could be shown that the gap width influences the dynamic of the flow, which could be seen in the measured bifurcation scenarios.

Then the effect of a rotating bottom plate was investigated. The stability diagram measured by Blohm and calculated by Mullin was compared with our calculation and shows a very good agreement. Both calculations showed a stability limit by decreasing the Reynolds number, which could not be found in the experiments due to a occuring time dependence.

The measurements to distinguish the growth of the bottom vortex show qualitatively a good agreement with our calculation. It could be pointed out that the effect depends on the value of Γ.

Indications for the onset of an oscillation were found in our numerical calculations by decreasing the Reynoldsnumber as much as in the experimental investigations of Blohm.

Now we focus our work on comparative experimental investigations with the new built setup and on numerical calculations for the full 3–D problem.

Acknowledgements. The financial support of Deutsche Forschungsgemeinschaft (DFG) is greatfully acknowledged. The authors want to thank Wolfgang Beyer, Rüdiger Maier and Klaus Franke for their assistance during this work.

References

1. Ahlers, G.: *Experiments on Bifurcations and One-Dimensional Patterns in Nonlinear Systems far from Equilibrium*; Complex Systems, SFI Studies in the Sciences of Complexity, Ed. D. Stein, Addison-Wesley Longman Publishing Group Ltd.,(1989)
2. Bänsch, E.: *Simulation of instationary incompressible flows*; Acta Math. Univ. Comenianae, volume [**LXVII**], pp101-114 (1998)
3. Benjamin, T. B.: *Bifurcation Phenomena in steady flows of a viscous fluid. I. Theory*; Proc. Roy. Soc. Lond., volume [**A359**], pp1-26 (1978)
4. Benjamin, T. B.: *Bifurcation Phenomena in steady flows of a viscous fluid. I. Experiments*; Proc. Roy. Soc. Lond., volume [**A359**], pp27-43(1978)
5. Blohm, C.: *Bifurcation Phenomena in Taylor-Couette flow with asymmetric boundary conditions*, diploma thesis, ZARM, University of Bremen, (1997)
6. Chossat, P.; Iooss, G.: *The Couette–Taylor Problem.* Applied Math. Sc., vol 102, Springer (1994)
7. Cliffe, K.A. and Mullin, T.: *A numerical and experimental study of the Taylor problem with asymmetric end conditions*, 6th Int. Symp. on Finite Element Method in flow problems, June 16-20, Antibes, France, (1986)
8. Bristeau, M.O.; Glowinski, R.; Periaux, J.: *Numerical methods for the Navier–Stokes equations. Application to the simulation of compressible and incompressible flows.* Computer Physics Report 6, 73–188 (1987)
9. Koschmieder, E.L.: *Bénard Cells and Taylor Vortices*; Cambridge University Press, Cambridge, England (1993)
10. Meyer-Spasche, R.: *Pattern Formation in Viscous Flow*; International Series of Numerical Mathematics, volume [**128**], Birkhäuser Verlag (1999)
11. Raffel, M., Willert C., Kompenhans J.: *Particle Image Velocimetry: A Practical Guide* Springer Verlag (1998)
12. Ruck, B.(Edt.): *Lasermethoden in der Strömungsmeßtechnik*, AT-Fachverlag Stuttgart, 1990

13. Ruelle, D. and Takens, F.: *On the nature of turbulence*; Commun. Math. Phys., volume [**20**], pp167-192 (1971)
14. Rumpf, M. and Schmidt, A. et. al.: *GRAPE, Graphics Programming Environment*; report no. 8, SFB 256 Bonn (1990)
15. Tagg, R.: *The Couette-Taylor Problem*; Nonlinear Science Today, volume[**4**], pp1-25 (1994)
16. Taylor, G.I.: *Stability of a viscous liquid contained between two rotating cylinders*; Phil.Trans., volume [**A223**], pp289-343 (1923)
17. Tenhaeff, M.: *Berechnung inkompressibler rotationssymmetrischer Strömungen elektrisch leitender Flüssigkeiten unter dem Einfluß von rotierenden Magnetfeldern.* Diploma thesis, University of Freiburg (1997)
18. Wulf, P.: *Untersuchungen zum laminar turbulenten Überschlag im konzentrischen Kugelspalt* Fortschrittberichte(VDI), Reihe 7, Nr.333 (1997)

Berichte aus der Technomathematik ISSN 1435-7968

http://www.math.uni-bremen.de/zetem/berichte.html

— Vertrieb durch den Autor —

Reports **Stand: 9. März 2000**

98–01. Peter Benner, Heike Faßbender:
An Implicitly Restarted Symplectic Lanczos Method for the Symplectic Eigenvalue Problem, Juli 1998.

98–02. Heike Faßbender:
Sliding Window Schemes for Discrete Least-Squares Approximation by Trigonometric Polynomials, Juli 1998.

98–03. Peter Benner, Maribel Castillo, Enrique S. Quintana-Ortí:
Parallel Partial Stabilizing Algorithms for Large Linear Control Systems, Juli 1998.

98–04. Peter Benner:
Computational Methods for Linear–Quadratic Optimization, August 1998.

98–05. Peter Benner, Ralph Byers, Enrique S. Quintana-Ortí, Gregorio Quintana-Ortí:
Solving Algebraic Riccati Equations on Parallel Computers Using Newton's Method with Exact Line Search, August 1998.

98–06. Lars Grüne, Fabian Wirth:
On the rate of convergence of infinite horizon discounted optimal value functions, November 1998.

98–07. Peter Benner, Volker Mehrmann, Hongguo Xu:
A Note on the Numerical Solution of Complex Hamiltonian and Skew-Hamiltonian Eigenvalue Problems, November 1998.

98–08. Eberhard Bänsch, Burkhard Höhn:
Numerical simulation of a silicon floating zone with a free capillary surface, Dezember 1998.

99–01. Heike Faßbender:
The Parameterized SR Algorithm for Symplectic (Butterfly) Matrices, Februar 1999.

99–02. Heike Faßbender:
Error Analysis of the symplectic Lanczos Method for the symplectic Eigenvalue Problem, März 1999.

99–03. Eberhard Bänsch, Alfred Schmidt:
Simulation of dendritic crystal growth with thermal convection, März 1999.

99–04. Eberhard Bänsch:
Finite element discretization of the Navier-Stokes equations with a free capillary surface, März 1999.

99–05. Peter Benner:
Mathematik in der Berufspraxis, Juli 1999.

99–06. Andrew D.B. Paice, Fabian R. Wirth:
Robustness of nonlinear systems and their domains of attraction, August 1999.

99–07. Peter Benner, Enrique S. Quintana-Ortí, Gregorio Quintana-Ortí:
Balanced Truncation Model Reduction of Large-Scale Dense Systems on Parallel Computers, September 1999.

99–08. Ronald Stöver:
Collocation methods for solving linear differential-algebraic boundary value problems, September 1999.

99–09. Huseyin Akcay:
Modelling with Orthonormal Basis Functions, September 1999.

99–10. Heike Faßbender, D. Steven Mackey, Niloufer Mackey:
Hamilton and Jacobi come full circle: Jacobi algorithms for structured Hamiltonian eigenproblems, Oktober 1999.

99–11. Peter Benner, Vincente Hernández, Antonio Pastor:
On the Kleinman Iteration for Nonstabilizable System, Oktober 1999.

99–12. Peter Benner, Heike Faßbender:
A Hybrid Method for the Numerical Solution of Discrete-Time Algebraic Riccati Equations, November 1999.

99–13. Peter Benner, Enrique S. Quintana-Ortí, Gregorio Quintana-Ortí:
Numerical Solution of Schur Stable Linear Matrix Equations on Multicomputers, November 1999.

99–14. Eberhard Bänsch, Karol Mikula:
Adaptivity in 3D Image Processing, Dezember 1999.

00–01. Peter Benner, Volker Mehrmann, Hongguo Xu:
Perturbation Analysis for the Eigenvalue Problem of a Formal Product of Matrices, Januar 2000.

00–02. Ziping Huang:
Finite Element Method for Mixed Problems with Penalty, Januar 2000.

00–03. Gianfrancesco Martinico:
Recursive mesh refinement in 3D, Februar 2000.

00–04. Eberhard Bänsch, Christoph Egbers, Oliver Meincke, Nicoleta Scurtu:
Taylor-Couette System with Asymmetric Boundary Conditions, Februar 2000.